First-Principles Study of the Structure and the Electronic Structure of Yttrium Aluminum Garnet Y3Al5O12

ARTICLE *in* INTERNATIONAL JOURNAL OF QUANTUM CHEMISTRY · AUGUST 2009

Impact Factor: 1.43 · DOI: 10.1002/qua.22030

3 AUTHORS, INCLUDING:

Ana B Munoz-Garcia
University of Naples Federico II
29 PUBLICATIONS **294** CITATIONS
SEE PROFILE

Luis Seijo
Universidad Autónoma de Madrid
160 PUBLICATIONS **3,805** CITATIONS
SEE PROFILE

First-Principles Study of the Structure and the Electronic Structure of Yttrium Aluminum Garnet $Y_3Al_5O_{12}$

ANA BELÉN MUÑOZ-GARCÍA,[1] EDUARDO ANGLADA,[2] LUIS SEIJO[1,3]

[1]*Departamento de Química, C-XIV, Universidad Autónoma de Madrid, 28049 Madrid, Spain*

[2]*Departamento de Física de la Materia Condensada, Universidad Autónoma de Madrid, 28049 Madrid, Spain*

[3]*Instituto Universitario de Ciencia de Materiales Nicolás Cabrera, Universidad Autónoma de Madrid, 28049 Madrid, Spain*

Received 27 October 2008; accepted 2 December 2008
Published online 12 March 2009 in Wiley InterScience (www.interscience.wiley.com).
DOI 10.1002/qua.22030

ABSTRACT: Density functional theory calculations have been performed on the electronic structure and the atomistic structure of yttrium aluminum garnet $Y_3Al_5O_{12}$, YAG, and related crystals (yttrium aluminum perovskite $YAlO_3$, yttria Y_2O_3, and corundum α-Al_2O_3). The quality of the computed data provides reliability to further structural studies with the same methods on local and extended bulk and surface defects in YAG. The structure of the computed conduction band is coherent with available electron-loss near-edge spectroscopy (ELNES) data. Previous Y-Al covalent interactions are not observed here. Reaction energies involving YAG and its related materials are given. Int J Quantum Chem 109: 1991–1998, 2009

Key words: YAG; first-principles; DFT; structure; thermodynamical data

Correspondence to: L. Seijo; e-mail: luis.seijo@uam.es
Contract grant sponsor: Ministerio de Educación y Ciencia, Spain (Dirección General de Investigación).
Contract grant number: CTQ2005-08550.
Contract grant sponsor: Comunidad de Madrid (Personal Investigador en Formación).

1. Introduction

Yttrium aluminum garnet $Y_3Al_5O_{12}$, or YAG, is an optical material of the utmost importance. The mechanical, thermal, and optical properties of this synthetic garnet have made it a practical choice for a range of applications, such as thermal coating, optical lenses, and widely used solid-state lasers and solid-state-lighting phosphors [1–3].

Despite its importance, the number of first-principles studies on this material is surprisingly small. The periodic boundary conditions (PBC) first-principles calculations we are aware of are limited to the density functional theory (DFT) calculations within the local density approximation (LDA) of Xu and Ching [4], the Hartree-Fock (HF) calculations of Shelyapina et al. [5], and the tight-binding linearized muffin-tin orbital LDA (TB-LMTO-LDA) calculations of Pari et al. [6]. Xu and Ching [4] computed the electronic structure, the lattice constant, and the bulk modulus, with a good agreement with experimental data; later, they made comparisons with and helped to interpret the electron energy loss near edge structure (ELNES) experiments [7]. However, they adopted the experimental relative atomic positions within the unit cell in their calculations and did not attempt the calculation of the YAG structure at the atomistic level. This task was not performed even in the more recent calculations of Pari et al. [6] and Shelyapina et al. [5] where even the lattice constant was fixed to experimental values.

The first-principles calculation of the structure of YAG at the atomistic level is the primary goal of this article. Being able to predict the structure of YAG at the atomistic level from the first-principles is very important because it is a necessary condition for the reliability of further calculations on local and extended bulk and surface defects in this material, whose structures are hard to get from experiments alone and are, nevertheless, key factors governing, for instance, the lasing and luminescence properties of YAG related materials, like YAG:Nd^{3+} and YAG:Ce^{3+} [3, 8] and the mechanism of Y segregation at the grain boundaries, directly related with the resistance to creep in high-temperature ceramic composites [9]. In this line, Freeman et al. [10] pointed out the crucial importance of the local environment of individual cations on the structure and energetics of garnet solid solutions. Besides, reliability of the local structures enhances reliability of the bonding analyses.

PBC first-principles atomistic structure predictions have been made in other garnets like pyrope, $Mg_3Al_2Si_3O_{12}$, at the HF level [11], and pyrope and grossular, $Ca_3Al_2Si_3O_{12}$, at the DFT level [10].

From the point of view of embedded-cluster first-principles calculations with quantum chemistry methods on YAG related materials, a recent attempt has been made on the computer simulation of the blue absorption and yellow luminescence of the solid-state lighting (SSL) phosphor YAG:Ce^{3+} [12]. The calculation provided reasonably good profiles of the absorption and luminescence spectra, but failed in an equally good description of the Stokes shift and pointed out the importance of the local atomistic structures in the ground state and in the excited states for light absorption and luminescence studies in YAG-related materials.

In the line of study of YAG related phosphors with application in SSL devices, like YAG:Ce^{3+}, some issues have been pointed out to be important, like codoping with Ga^{3+} and La^{3+} [13] producing single-crystalline films [14] or controlling the antisite defect concentration [15]. This work belongs to a first-principles line of approach to the problem started in our lab [12] and represents the first step toward and exploitation of accurate and efficient PBC methods for structural calculations [16, 17] and their link with state-of-the-art embedded-cluster methods for luminescence simulations [12].

We present the details of the calculations in Section 2, and we discuss the results in Section 3.

2. Details of the Calculations

The first-principles calculations in this article have been performed with the periodic boundary conditions self-consistent SIESTA method [16, 17], using density functional theory [18, 19] (DFT) within the generalized gradient approximation (GGA) as formulated by Perdew, Burke, and Ernzerhof [20, 21] (PBE). Norm-conserving pseudopotentials [22] in the Kleinman-Bylander form [23] have been generated for the following atoms and reference configurations: Y($5s^2\,4p^6\,4d^1$), Al ($3s^2\,3p^1$), and O ($2s^2 2p^4$), with nonlinear partial-core corrections [24] and semi-core states to account for large corevalence overlap in the case of Y. Atomic basis sets of a double-ξ plus polarization quality have been optimized for the three atoms by the fictitious enthalpy method of Anglada et al. [25] in an idealized cubic $YAlO_3$ perovskite, with the following sizes: Y($5s5s'4p4p'5p4d4d'$), Al($3s3s'3p3p'3d$), and

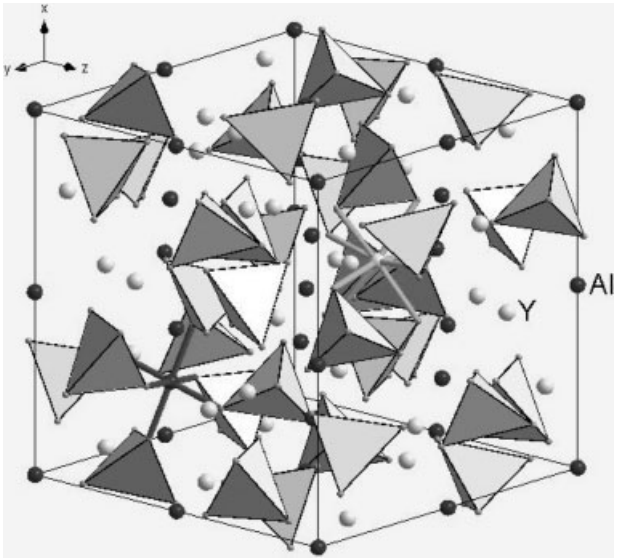

FIGURE 1. Unit cell of YAG. The yttrium ions, the aluminum ions in quasioctahedral sixfold coordinations, and the AlO_4 quasitetrahedral moieties are indicated.

O(2*s*2*s*′2*p*2*p*′3*d*). The charge density is projected on a uniform grid in real space, with an equivalent plane-wave cutoff of 380 Ry, to calculate the exchange-correlation and Hartree matrix elements. Total energy calculations have been converged with respect to k-space integration; a k grid cutoff of 15.0 Bohr was used.

All geometry optimizations have been performed without imposing any symmetry restrictions in the position of all atoms in the unit cell, using a conjugate gradient method, with a force tolerance of 0.04 eV/Å. Starting geometries were generated using the experimental information on the structure of YAG [26], according to which a unit cell of YAG contains eight formula units ($Y_3Al_5O_{12}$), with 160 atoms/cell (see Fig. 1); it belongs to Ia3*d* (230) space group, with Y in 24(*c*) 8fold coordinated sites, Al in 16(*a*) 6fold coordinated and 24(*d*) 4fold coordinated sites, and O in 96(*h*) sites; Y and Al sites are fixed within the unit cell, and O sites have three degrees of freedom (*x*, *y*, *z*).

3. Results and Discussion

The total energy per unit cell of the YAG crystal was calculated for a number of values of the lattice constant *a* and it is shown in Figure 2, together with the extracted P-V dependence. For each value of *a*, the positions of all the 160 unit cell atoms were optimized without any symmetry restrictions; the results showed that the original symmetry of the crystal was kept, so that all the optimized atomic

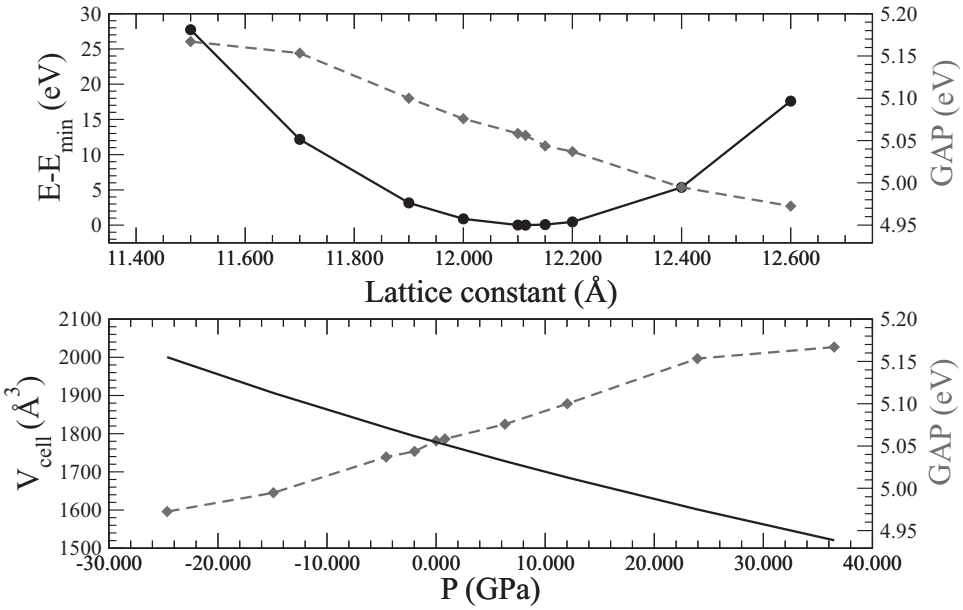

FIGURE 2. Upper graph: Calculated total energy per unit cell (full line; left axis) and band gap (dashed line; right axis) as functions of the lattice constant a. Lower graph: Calculated unit cell volume (full line; left axis) and band gap (dashed line; right axis) as functions of the internal pressure.

TABLE I

Structural data of YAG ($Y_3Al_5O_{12}$), YAP ($YAlO_3$), Yttria (Y_2O_3), and Corundum (αAl_2O_3).

		YAG ($Y_3Al_5O_{12}$) [230 Ia$\bar{3}$d; O 96(h)]											
		a(Å)	*x*(O)	*y*(O)	*z*(O)								
LDA	Ref. [4]	11.904	–	–	–								
LDA	This work	11.691	−0.0290	0.0510	0.1499								
PBE	This work	12.114	−0.0306	0.0519	0.1491								
Exp.	Ref. [26]	12.000	−0.0306	0.0512	0.1500								
		YAP ($YAlO_3$) [62 Pbnm; Y 4(*c*); O_I 4(c); O_{II} 8(d)]											
		a(Å)	*b*(Å)	*c*(Å)	*b*/*a*	*c*/*a*	*x*(Y)	*y*(Y)	*x*(O_I)	*y*(O_I)	*x*(O_{II})	*y*(O_{II})	*z*(O_{II})
PBE	This work	5.210	5.359	7.427	1.029	1.425	−0.013	0.051	0.087	0.476	−0.297	0.290	0.048
Exp.	Ref. [27]	5.178	5.328	7.367	1.029	1.422	−0.010	0.053	0.086	0.475	−0.297	0.293	0.044
		Yttria (Y_2O_3) [206 Ia$\bar{3}$; Y_{II} 24(d); O 48(e)]											
		a(Å)	*x*(Y_{II})	*x*(O)	*y*(O)	*z*(O)							
PBE	This work	10.405	−0.034	0.393	0.152	0.379							
Exp.	Ref. [28]	10.607	−0.032	0.392	0.151	0.380							
		Corundum (α-Al_2O_3) [167 R$\bar{3}$ c (hexagonal axes); Al 12(c); O 48(e)]											
		a(Å)	*c*(Å)	*c*/*a*	*z*(Al)	*x*(O)							
PBE	This work	4.812	13.092	2.721	0.353	0.311							
Exp.	Ref. [29]	4.760	12.993	2.729	0.352	0.308							

Spatial groups and special positions are indicated. The calculations in this work were not forced to maintain the indicated spatial group symmetries.

positions can be described with the structural data shown in Table I. In this Table, we include computed structural data for the YAG-related crystals yttrium aluminum perovskite $YAlO_3$ (YAP), Y_2O_3 (yttria), and α-Al_2O_3 (corundum), which were obtained in an equivalent manner. Table II shows the corresponding bulk moduli and the pressure derivatives as obtained from a fitting of the Murnaghan isothermic equation of state [45] to the computed energy-volume data. The results of the present DFT GGA calculation with the PBE functional agree very well with all the structural data, which supports its use in further structural studies of defects in YAG.

The PBE band structure of YAG computed at the theoretically determined structure is shown in Figure 3, where a direct band gap at Γ of 5.0 eV is observed, 22% smaller than the optical experimental value of 6.4 eV [46], which is a type of deviation expected for a GGA DFT calculation. This PBE value compares favorably with the 4.71 eV of the LDA calculation in Ref. 4 and the 1.4 eV of the TB-LMTO calculation in Ref. 6. As in the previous calculations [4, 6], the highest valence bands have basically no dispersion. In contrast with the observation made in Ref. [4], according to which the conduction band (CB) edge at Γ is made of two well-separated bands, we find the CB edge made of a simple band, of a main Y (4d + 5s) character. The pressure dependence of the gap is also shown in Figure 2. It shows a linear behavior up to 20 GPa, with slope 0.0041 eV/GPa, which is six times smaller than the 0.025 eV/GPa previously calculated by Xu and Ching [4].

Total and projected density of states (DOS) plots are shown in Figure 4. The orbitals with a dominant character of Y-4*p* appear at −20 eV and those of O-2*s* around −16 eV. The valence band (VB) extends over a 6 eV region, and it is very much dominated by the O-2*p* orbitals The bottom of the CB is dominated by the Y-5s and 4d orbitals, which extend over an energy region 5 eV wide. Above that, the CB has almost pure Al character, with even contributions from the octahedrally (Al_{oct}) and tetrahedrally (Al_{tet}) coordinated ones.

Orbital projected DOS are known to be able to give a first line of interpretation of electron-loss near-edge spectroscopy (ELNES), which are available for YAG [47]. For instance, the experimental Al $L_{2,3}$ near-edge (shown in Fig. 7 of Ref. [47]) is related with the Al($s + d$) PDOS (shown here in Fig. 5) because of the $\Delta l = \pm 1$ dipole selection rule

TABLE II

Bulk moduli of YAG, YAP, Yttria, and Corundum, and their first pressure derivatives.

		B (GPa)	*dB/dP*
	YAG		
PP-SM[a]	Ref. [30]	220.0	–
PP-SM[a]	Ref. [31]	198.0	–
LDA	Ref. [4]	220.7	4.12
PBE	This work	221.0	3.09
Experiment	Ref. [32]	220.0	–
Experiment	Ref. [33]	180.0	4.42
	YAP		
TB-LTMO-LDA[b]	Ref. [34]	218.4	–
LDA	Ref. [35]	234	3.75
GGA	Ref. [36]	188	3.82
PBE	This work	207.1	7.85
Experiment	Ref. [37]	204.9	–
Experiment	Ref. [38]	192	7.3
	Yttria		
LDA	Ref. [39]	183	4.01
PBE	This work	189.2	2.76
Experiment	Ref. [40]	170	–
	Corundum		
TB-LTMO-LDA[b]	Ref. [34]	265.8	–
HF	Ref. [41]	243.8	4.305
LDA	Ref. [42]	242	3.24
PBE	This work	234.6	4.48
Experiment	Ref. [43]	254	–
Experiment	Ref. [44]	254.4	4.275

[a] Shell-model pair potential method.
[b] Tight-binding method.

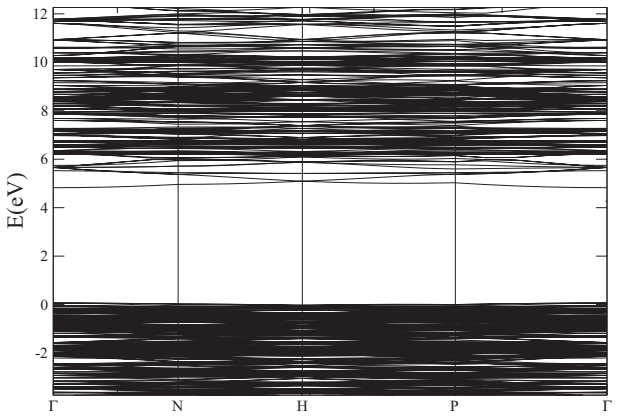

FIGURE 3. Energy bands of YAG as resulting from the DFT PBE calculation.

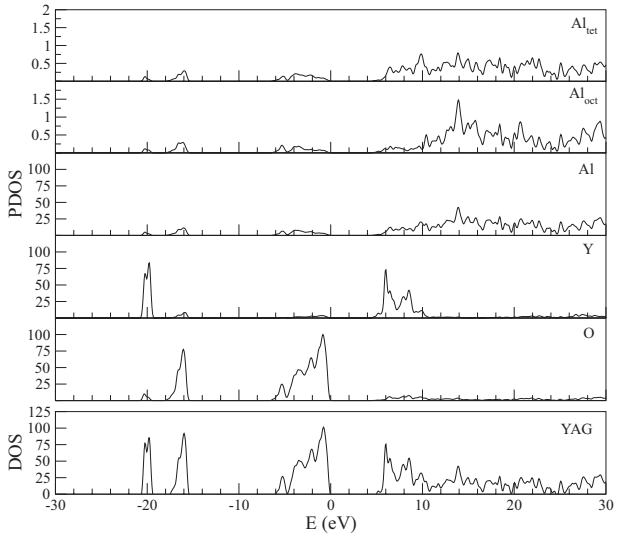

FIGURE 4. Calculated density of states of YAG and projected densities of states of the atoms of the unit cell O, Y, and Al, and of individual Al atoms with four-fold (Al_{tet}) and sixfold (Al_{oct}) coordinations.

governing the core electron excitations involved in ELNES. A comparison of both shows an acceptable agreement in the significant features and a poorer agreement of the relative intensities, which depend on the relative values of the transition moments [7]. The Al $L_{2,3}$ ELNES feature A at around 8 eV can be identified here with a peak starting at 6 eV, which is almost entirely due to Al_{tet}, not shown in previous

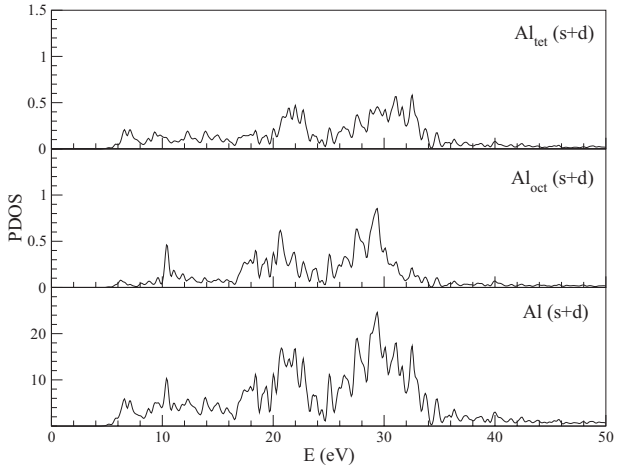

FIGURE 5. Calculated PDOS of the *s* and *d* unoccupied orbitals of all the Al atoms in the unit cell, Al (s + d), and of individual Al atoms with four-fold and six-fold coordinations, Al_{tet} (s + d) and Al_{oct}(s + d).

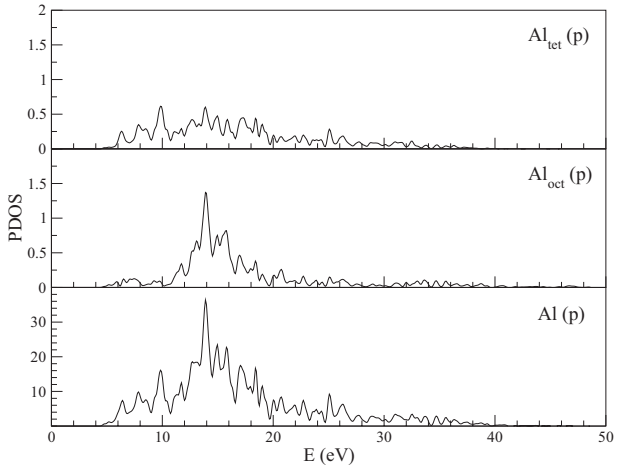

FIGURE 6. Calculated PDOS of the *p* unoccupied orbitals of all the Al atoms in the unit cell, Al(p), and of individual Al atoms with four-fold and six-fold coordinations, Al_{tet} (p) and Al_{oct} (p).

calculations [4, 7, 47]. The sharp ELNES feature B at 13 eV seems to correspond with the PDOS peak just under 11 eV, due to Al_{oct}. Features C and D between 14 and 18 eV correspond with similar features in the PDOS at almost the same energies, the second one with a marked Al_{oct} character. The E feature around 22 eV is shown here at the same energy with its initial and final parts having Al_{oct} and Al_{tet} characters, respectively. The F feature cannot be clearly distinguished here. Finally, the marked G feature more than 10 eV wide peaking at 34 eV appears here shifted at lower energies (peaking at almost 30 eV) and not so wide (10 eV wide). It is preceded by a valley which shows up in the PDOS.

Similarly, the experimental Al *K* near-edge (shown in Fig. 9 of Ref. [47]) is related with the Al(*p*) PDOS (shown here in Fig. 6) The ELNES features are also shown in the PDOS diagram, although with a rather systematic underestimation of the energies: The prominent C peak at 18 eV is shown in the PDOS at 14 eV, almost entirely due to Al_{oct}; the B shoulder between 12 and 14 eV corresponds with the PDOS peak at 10 eV, due to Al_{tet}; and the D shoulder between 20 and 22 eV with the 17–9 eV PDOS features and the E prominence between 26 and 28 eV with the 25–27 eV PDOS features, both of them due to both Al_{oct} and Al_{tet}.

Finally, the experimental Y $L_{2,3}$ near-edge (shown in Fig. 5 of Ref. [47]) shows a single wide peak centered at 9 eV, which corresponds with the

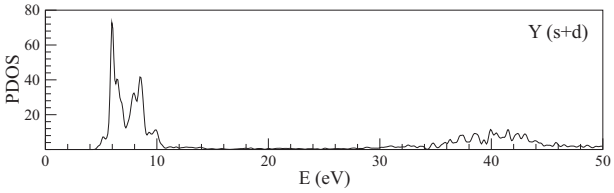

FIGURE 7. Calculated PDOS of the s and d unoccupied orbitals of all the Y atoms in the unit cell.

Y (*s* + *d*) PDOS features (shown here in Fig. 7) which extend from 5 to 11 eV.

The picture of the chemical bond in YAG as given by the Mulliken population analysis [48] is that of covalent interactions within the AlO_4 moieties, less covalent interactions between Al_{oct} and its surrounding oxygens, and pretty ionic interactions between Y and the lattice. The Mulliken effective ionic charges of YAG are shown in Table III, together with those of related crystals. Y seems to be more ionic in YAG than in Y_2O_3, and the charges of O and Al are far from the ionic limit. Overlap populations are 0.23 for Al_{oct}-O (at 1.948 Å) and 0.34 for Al_{tet}-O (at 1.788 Å), slightly larger than the values of α-Al_2O_3, 0.22 and 0.17, at 1.855 and 1.972 Å, respectively. Overlap populations for Y—O are low, 0.02–0.03, slightly smaller than the values in Y_2O_3, of around 0.06. The O—O overlap populations are very low in all cases and sometimes negative, which means that they are not meaningful and O—O bonding interactions are not relevant in these materials according to the present calculations. Finally, the overlap populations between Y and Al are negligible, both Y-Al_{oct} and Y-Al_{tet}, so that our calculations do not support the suggestions of Ref. 4, according to which Y and Al_{tet} may interact covalently in spite of the fact that they are both cations.

TABLE III

Mulliken effective ionic charge of YAG, YAP, Yttria, and Corundum.

	YAG	YAP	Yttria	Corundum
O	−0.96	−0.99 −1.00	−1.33	−0.91
Y	+2.33	+2.27	+2.01 (S_6) +1.99 (C_2)	
Al	+0.99 (oct) +0.83 (tet)	+0.72		+1.36

TABLE IV

Reaction enthalpies at zero pressure involving YAG, YAP, Yttria, and Corundum.

a	$3Y_2O_3 + 5Al_2O_3 \rightleftharpoons 2Y_3Al_5O_{12}$	$\Delta H = -7.39$ eV
b	$Al_2O_3 + 3YAlO_3 \rightleftharpoons Y_3Al_5O_{12}$	$\Delta H = +0.64$ eV
c	$Y_2O_3 + Al_2O_3 \rightleftharpoons 2YAlO_3$	$\Delta H = -2.89$ eV

We have also calculated reaction energies involving Yttria, Corundum, YAP, and YAG, out of the total energies per unit cell of the four individual crystals. For this purpose, we use total energies that are converged with respect to the numerical grid. The results are shown in Table IV. Note that reaction energies coincide with reaction enthalpies at zero pressure. There are no experimental data available to check with, as far as we know. The only previous theoretical results we are aware of are the shell-model pair potential simulations of Ref. [49], which are reported to be -4.8 eV, -1.6 eV, and -0.1 eV, respectively, for reactions a, b, and c in Table IV; these results have the problem that they are not consistent with the condition $\Delta H_a - 2\Delta H_b - 3\Delta H_c = 0$, which makes difficult to make direct comparisons. Our results picture YAP and YAG with a very similar energetic stability, so that their relative stability must be controlled by the entropy factor.

4. Conclusions

First-principles DFT GGA calculations with the PBE functional have been made on the electronic structure and the atomistic structure of YAG, with a unit cell of 160 atoms, and of YAG-related crystals (YAP, yttria, and corundum). The computed structural data (lattice constants and atomic positions within the unit cell without symmetry restrictions) agree very well with experiments, which provides the necessary reliability for further structural studies on local and extended bulk and surface defects in YAG, which determine many of the interesting properties of doped YAG materials and have a limited experimental accessibility. Band structure calculations reveal an acceptable underestimation of the YAG band gap and the structure of the conduction band is coherent with the available ELNES experimental data. Also, first-principles thermodynamical data are given on the reaction energies between YAG ($Y_3Al_5O_{12}$), YAP ($YAlO_3$), yttria (Y_2O_3) and corundum (α-Al_2O_3).

References

1. deWith, G. In High Technology Ceramics; Vincenzini, P., Eds.; Elsevier: Amsterdam, 1987, p 2063.
2. Powell, R. C. Physics of Solid State Laser Materials; AIP: New York, 1998.
3. Justel, T.; Nikol, H.; Ronda, C. Angew Chem Int Ed 1998, 37, 3085.
4. Xu, Y-N.; Ching, W. Y. Phys Rev B 1999, 59, 10530.
5. Shelyapina, M. G.; Kasperovich, V. S.; Wolfers, P. J. Phys Chem Solids 2006, 67, 720.
6. Pari, G.; Mookerjee, A.; Bhattacharya, A. K. Phys B 2005, 365, 163.
7. Xu, Y-N.; Chen, Y.; Mo, S. D.; Ching, W. Y. Phys Rev B 2002, 65, 235105.
8. Blasse, G.; Bril, A. J Chem Phys 1967, 47, 5139.
9. Wang, C. M.; Cargill, G. S.; Harmer, M. P.; Chan, H. M.; Cho, J. Acta Mater 1999, 47, 3411.
10. Freeman, C. L.; Allan, N. L.; van Westrenen, W. Phys Rev B 2006, 74, 134203.
11. D'Arco, P.; Fava, F. F.; Dovesi, R.; Saunders, V. R. J Phys: Condens Matter 1996, 8, 8815.
12. Gracia, J.; Seijo, L.; Barandiarán, Z.; Curulla, D.; Niemans-verdriet, H.; van Gennip, W. J Lumin 2008, 128, 1248.
13. Pan, Y.; Wu, M.; Su, Q. J Phys Chem Solids 2004, 65, 845.
14. Zorenko, Y.; Gorbenko, V.; Konstankevych, I.; Voloshinovskii, A.; Stryganyuk, G.; Mikhailin, V.; Kolobanov, V.; Spassky, D. J Lumin 2005, 114, 85.
15. Zhao, G. J.; Zeng, X. H.; Xu, J.; Zhou, S. M.; Zhou, Y. Z. Phys Status Solidi A 2003, 199, 355.
16. Ordejón, P.; Artacho, E.; Soler, J. M. Phys Rev B 1996, 53, 10441.
17. Soler, J.; Artacho, M. E.; Gale, J. D.; García, A.; Junquera, J.; Ordejón, P.; Sánchez-Portal, D. J Phys: Condens Matter 2002, 14, 2745.
18. Kohn, W.; Sham, L. J Phys Rev 1965, 140, 1133.
19. Hohenberg, P.; Kohn, W. Phys Rev B 1964, 136, 864.
20. Perdew, K. B. J. P.; Ernzerhof, M. Phys Rev Lett 1996, 77, 3865.
21. Perdew, K. B. J. P.; Ernzerhof, M. Phys Rev Lett 1997, 78, 1396.
22. Troullier, N.; Martins, J. L. Phys Rev B 1991, 43, 1993.
23. Kleinman, L.; Bylander, D. M. Phys Rev Lett 1982, 48, 1425.
24. Louie, S. F. S. G.; Cohen, M. Phys Rev B 1982, 26, 1738.
25. Anglada, E.; Soler, J. M.; Junquera, J.; Artacho, E. Phys Rev B 2002, 66, 205101.
26. Euler, F.; Bruce, J. A. Acta Crystallogr 1965, 19, 971.
27. Diehl, R.; Brandt, G. Mater Res Bull 1975, 10, 85.
28. Faucher, M.; Pannetier, J. Acta Crystallogr B 1980, 36, 3209.
29. Lewis, J.; Schwarzenbach, D.; Flack, H. D. Acta Crystallogr A 1982, 38, 733.
30. Bush, T. S. J.; Gale, C.; Catlow, R. A.; Battle, P. D. J Mater Chem 1994, 4, 831.
31. Kuklja, M.; Pandey, R. J Am Chem Soc 1999, 82, 2881.
32. Hofmeiser, A. M.; Campbell, K. R. J Appl Phys 1992, 72, 638.

33. Yogurtcu, Y. K.; Miller, A. J.; Saunders, G. A. J Phys C 1980, 13, 6585.
34. Pari, G.; Mookerjee, A.; Bhattacharya, A. K. Phys B 2004, 353, 192.
35. Ching, W. Y.; Xu, Y. N. Phys Rev B 1999, 59, 12815.
36. Wu, X.; Qin, S.; Wu, Z. J Phys: Condens Matter 2006, 18, 3907.
37. Ross, N. Phase Trans 1996, 58, 27.
38. Ross, J. N. L.; Angel, R. J Solid State Chem 2004, 17, 1276.
39. Xu, Y-N.; Gu, Z.; Ching, W. Y. Phys Rev B 1997, 56, 14993.
40. Manning, O. H. W. R.; Powell, B. J Am Chem Soc 1969, 52, 436.
41. Boettger, J. C. Phys Rev B 1996, 55, 750.
42. Ching, W. Y.; Xu, Y. N. J Am Chem Soc 1994, 77, 404.
43. Goto, I.; Anderson, O. T. O. L.; Yamamoto, S. J Geophys Res 1989, 94, 7588.
44. d'Amour, H.; Schiferl, D.; Denner, W.; Schulz, H.; Holzapfel, B. J Appl Phys 1978, 49, 4411.
45. Murnagan, F. D. Proc Natl Acad Sci USA 1944, 30, 244.
46. Slack, G. A.; Oliver, D. W.; Chrenko, R. M.; Roberts, S. Phys Rev 1969, 177, 1308.
47. Gülgün, M. A.; Ching, W-Y.; Xu, Y-N.; Rühle, M. Phil Mag B 1999, 79, 921.
48. Mulliken, R. S. J Chem Phys 1955, 23, 1933.
49. Kuklja, M. J Phys: Condens Matter 2000, 12, 2953.